Compensation for temperature-dependent phase and velocity of guided wave signals for structural health monitoring

(Article begins on next page)

20 November 2024

Compensation for temperature dependent phase and velocity of guided wave signals in baseline subtraction for SHM

Stefano Mariani, Sebastian Heinlein, Peter Cawley

Imperial College London, Exhibition Road, South Kensington, London SW7 2AZ, UK

Abstract

Baseline subtraction is commonly used in guided wave SHM to identify the signal changes produced by defects. However, before subtracting the current signal from the baseline it is essential to compensate for changes in environmental conditions such as temperature between the two readings. This is often done via the baseline stretch method that seeks to compensate for wave velocity changes with temperature. However, the phase of the signal generated by the transduction system is also commonly temperature sensitive and this effect is neglected in the usual compensation procedure. This paper presents a new compensation procedure that deals with both velocity and phase changes. The results with this new method have been compared with those obtained using the standard baseline stretch technique on both a set of experimental signals and a series of synthetic signals with different coherent noise levels, feature reflections and defect sizes, the range of noise levels and phase changes being chosen based on initial experiments and prior field experience. It has been shown that the new method both reduces the residual signal from a set baseline and enables better defect detection performance than the conventional baseline signal stretch method under all conditions examined, the improvement increasing with the size of the temperature and phase differences encountered. For example, in the experimental data, the new method roughly halved the residual between baseline and current signals when the two signals were acquired at temperatures 15 °C apart.

Introduction

Ultrasonic guided wave inspection has recently become common practice in some large structures due to its ability to test large areas from a single sensor location [1]. One application in which it has been successfully applied is testing of pipes in the oil and gas industry [2], where typically the first order torsional wave mode is employed in a pulse-echo configuration at frequencies in the order of tens of kHz. This wave mode offers advantages such as a virtually uniform coverage of the entire pipe-wall and a very low attenuation in steel, which enables inspection for tens of meters from the sensor location [3]. The drawback is a reduced sensitivity to changes in the pipe cross section, particularly when the guided wave sensors are used in a one-off inspection configuration. In this setting the defect 'call level' is typically set to reflection amplitudes corresponding to defects that present approximately 5% change in the cross-sectional area of the pipe [4]. This value can vary significantly depending on the general condition of the inspected pipe, the position of the defect and the presence of other pipe features, such as welds, that also give reflections [5]. Furthermore, in addition to the desired torsional wave mode, other

1

signal components exist due to the excitation and reception of unwanted modes and imperfect direction control [2]. Because these components are deterministic they cannot be eliminated through averaging and hence they set a background noise level which is referred to as coherent noise. Defects must produce a reflection somewhat larger than this noise for reliable detection in a one-off inspection.

Driven by the need to increase the defect sensitivity and to reduce the high costs of gaining access to some test locations, there has recently been a move towards permanent installation of sensors. This allows the system to be operated in a monitoring configuration [5], so baseline subtraction techniques can be used [6]. Typically, a first inspection is performed when the pipe (or, generally, the structure of interest) is in a known structural condition, and that measurement is stored and labeled as 'baseline'. The baseline can then be subtracted from any later measurement to highlight changes in the structure response. While this procedure theoretically enables a much greater sensitivity, difficulties arise as changing environmental and operational conditions (EOCs) also cause changes in the wave propagation. A possible solution to this problem would be the early collection of a large number of baselines acquired under different EOCs, followed by selection of the best one to subtract from any later reading, in a procedure called optimal baseline selection (OBS) [7,8]. Unfortunately, such a solution is often impractical as a very large number of baseline signals are required at small variations of operating condition [9].

Temperature is a very common cause of signal variation as the guided wave velocity is a significant function of temperature [9–11]. As a result, the arrival time of the reflections from features in the pipe varies, leading to imperfect baseline subtraction. To compensate for this effect a well-established technique called baseline signal stretch (BSS) was proposed by several authors [7,9,12]. The idea is to compress or dilate the signal by some stretch factor that minimizes the residuals. Harley and Moura recently discussed computational aspects of the BSS procedure and proposed a new computationally efficient algorithm making use of the scale transform domain [13]. While the BSS approach works relatively well for small temperature differences between the baseline and any later reading, the performance deteriorates as the temperature difference increases. The main reason for this is that the BSS method only targets the propagation speed change, neglecting other indirect effects on the wave propagation caused by temperature variations. For example, when the temperature changes, the bonding stiffness at the interface between the transducers and the structure is likely to vary, leading to frequency response changes that can affect both the amplitude and the phase of the signal [9,14]. Furthermore, if the system is operated close to resonance, ringing may be seen at some temperatures. Similar phenomena are also seen with EMAT based systems [15,16].

However, there is only a small amount of work in the literature on quantifying and possibly compensating for transducer electro-mechanical response variations [16–19]. Assous et al. [17] measured the magnitude and phase response at different frequencies (but at constant temperature) of wideband piezoelectric transducers employed in a pitch-catch arrangement, and proposed a compensation procedure whereby the excitation signal was digitally inverse filtered

in order to improve the bandwidth. Hurst et al. [18] reached a similar goal by developing a specialized analog filter applied to the measured ultrasonic signal that compensates for the transducer transfer function at different frequencies. While this compensation procedure did include a fine-tuning to compensate for temperature effects, the drawback is that real-time analog filtering only allows causal filtering, which results in small time delays of the signals. In medical ultrasound, Labyed and Huang [19] developed an experimental method to estimate the phase response of transducer elements at different frequencies using measured signals scattered from a glass microsphere embedded in a tissue-mimicking phantom and proposed a modified imaging algorithm that improved the achievable resolution by accounting for the measured phase response. The drawback of these methods is that they need calibration or some a-priori knowledge of the transducer behavior. Recently, Herdovics and Cegla [16] proposed an iterative temperature and phase compensation method capable of compensating for both the transducer phase response change and the wave propagation speed change. The advantage of the method is that it only uses the ultrasonic signals themselves, without the need for any knowledge of the sensor characteristics; the drawback is that at least two sensors installed at two different locations of the structure are needed to carry out the iterative procedure (i.e. systems performing measurements in a pulse-echo arrangement are excluded).

A potential concern with any method of compensation for environmental changes involving minimization of residuals between the current signal and a baseline is that, when the measurement is recorded from the structure in a damaged state, the procedure used to modify the signal can also reduce the residuals produced by the signal component reflected by the anomaly, therefore hindering the defect detection. To the authors' knowledge, this potential difficulty has not been addressed in the literature.

This paper has two purposes. First, a novel temperature compensation method is presented which seeks to compensate for both wave propagation speed change and transducer phase response change, which is particularly valuable when large temperature differences between the baseline and later measurements are expected. The method provides estimates of both phase shift and propagation speed change solely from the baseline and subsequent signals, and it is also well suited for pulse-echo systems. Although the proposed method is presented here as applied to a guided wave pipe inspection system employing the first order torsional mode, it is believed to be applicable to other types of guided wave inspection systems employing a single, non-dispersive mode, as well as to ultrasonic systems using bulk waves. The second aim of the paper is to investigate the extent to which using a method that seeks to modify a measurement in order to minimize its residual with respect to a baseline signal (such as the method presented here or the standard BSS technique) can reduce detectability by minimizing the change produced by the defect.

The paper is structured as follows. In the next section, the proposed temperature compensation method is presented and applied to simulated torsional guided wave signals in pipes. The following section compares the results with the new method to those obtained with the standard

baseline stretch method on an experimental data set. This is followed by derivation of receiver operating characteristic (ROC) curves [20] for both the conventional and new techniques on synthetic signals with different coherent noise levels, defect sizes and feature reflections. The final section gives the main conclusions of the study.

Proposed temperature compensation method

The negative effects caused by variations of the transducer phase response at different temperatures on the performance of the BSS method, as well as an enhanced method designed to mitigate this issue, are illustrated in this section with the aid of finite element (FE) simulations. The FE solver used to perform the analyses discussed in this section and throughout the whole paper is POGO [21]. A 7 meter long section of an 8 inch schedule 40 pipe was discretized with 2 mm characteristic length hexahedral elements, and a simulated sensor ring was positioned 3 m away from one of the pipe ends. The direction of interest for wave propagation is the forward direction as seen in Figure 1. With the pipe in the backward direction being longer and free of features, the reflections from all the features in the forward direction were seen before the reflection from the pipe end in the backward direction so it was not necessary to model the direction control system used in practical testing [2]. Two welds were modeled as thickness increases, each with a length of 8 mm and a height of 2 mm, starting at distances of 0.6 and 1.8 m from the source of guided waves, as depicted in Figure 1. To simulate the sensor ring, 26 nodes equally spaced around the pipe external circumference were selected and were used to produce tangential forces and to sense tangential displacements, thus generating and receiving the T(0,1) mode [22,23].
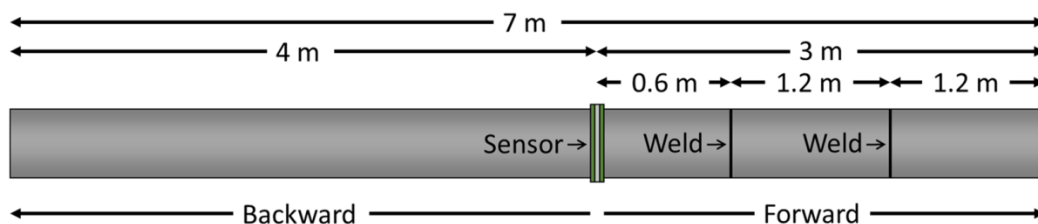

Figure 1. Dimensions of the modeled 8 inch schedule 40 pipe used in the analysis of section "Proposed temperature compensation method"

Figure 2 shows signals obtained from simulations with the pipe at 20 °C and 50 °C, the effect of temperature being modelled via a change in shear modulus, Poisson's ratio and density to give T(0,1) wave speeds of 3249.3 m/s and 3235.2 m/s at the two temperatures respectively, these values being obtained from the experiments described in the next section. The excitation signal was an 8 cycle, 25.5 kHz Hanning windowed toneburst and its phase was advanced by 120° at the higher temperature, this value being representative of the phase changes seen experimentally. Because of the slower wave speed at the higher temperature, the 50 °C signal in Figure 2(a) shows delayed arrivals of the reflections from the pipe features when compared to the 20 °C signal in the same figure. This is better shown in the zoomed plot of Figure 2(b), where the

envelope of the pipe end reflection at 50 °C is clearly delayed respect to the one at 20 °C (even if, due to the different signal phases, by looking at the RF peaks the 50 °C signal might appear to arrive earlier than the 20 °C one).
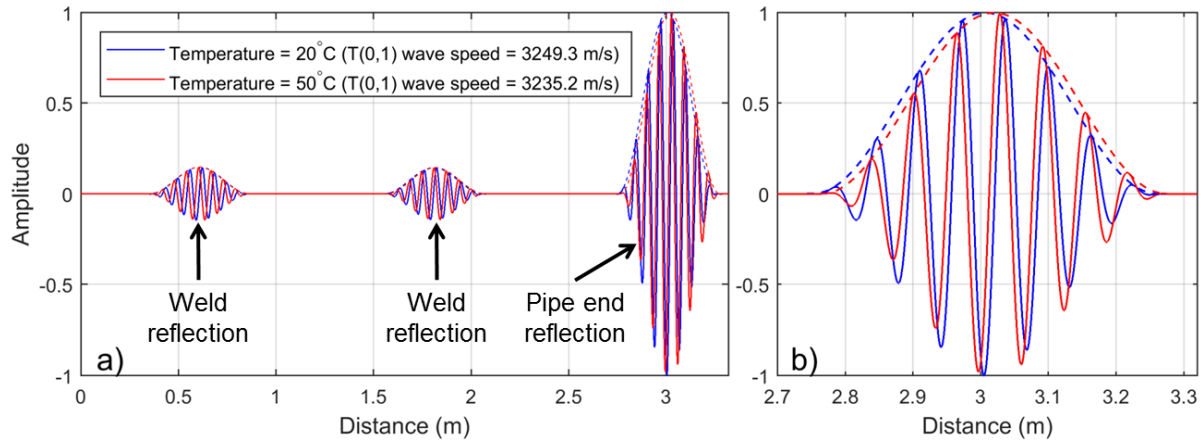

Figure 2. Simulated torsional guided wave signals traveling in the "forward" direction of the modeled pipe of Figure 1 ((b) Zoom on the reflections from the end of the pipe). Two different pipe temperatures of 20 °C and 50 °C were modeled: the ratio between the two wave speeds is ~1.0043 and the phase of the excitation signal at 50 °C was advanced by 120°. Distances are measured from the center of the transmitted toneburst.

Figure 3(a-b) shows the signals and corresponding envelopes obtained when using the standard BSS method [13] on the signals displayed in Figure 2. The signal at 20 °C was used as the baseline, and the signal at 50 °C was stretched in time. The zoomed plot in Figure 3(b) shows the wave packet reflected from the end of the pipe. This shows how the BSS method correctly aligns the peaks of the RF signal to minimize the residuals. However, the envelopes are misaligned, due to the different phase of the input tonebursts. As a result, the computed stretch factor of ~0.9973 is not the "true" stretch factor, which is the ratio between the T(0,1) wave speeds at the two temperatures, namely ~1.0043. Therefore, in this case, although it was expected that the signal at 50 °C would be compressed in time to compensate for the slower torsional wave speed, the residual was minimized by it being dilated.
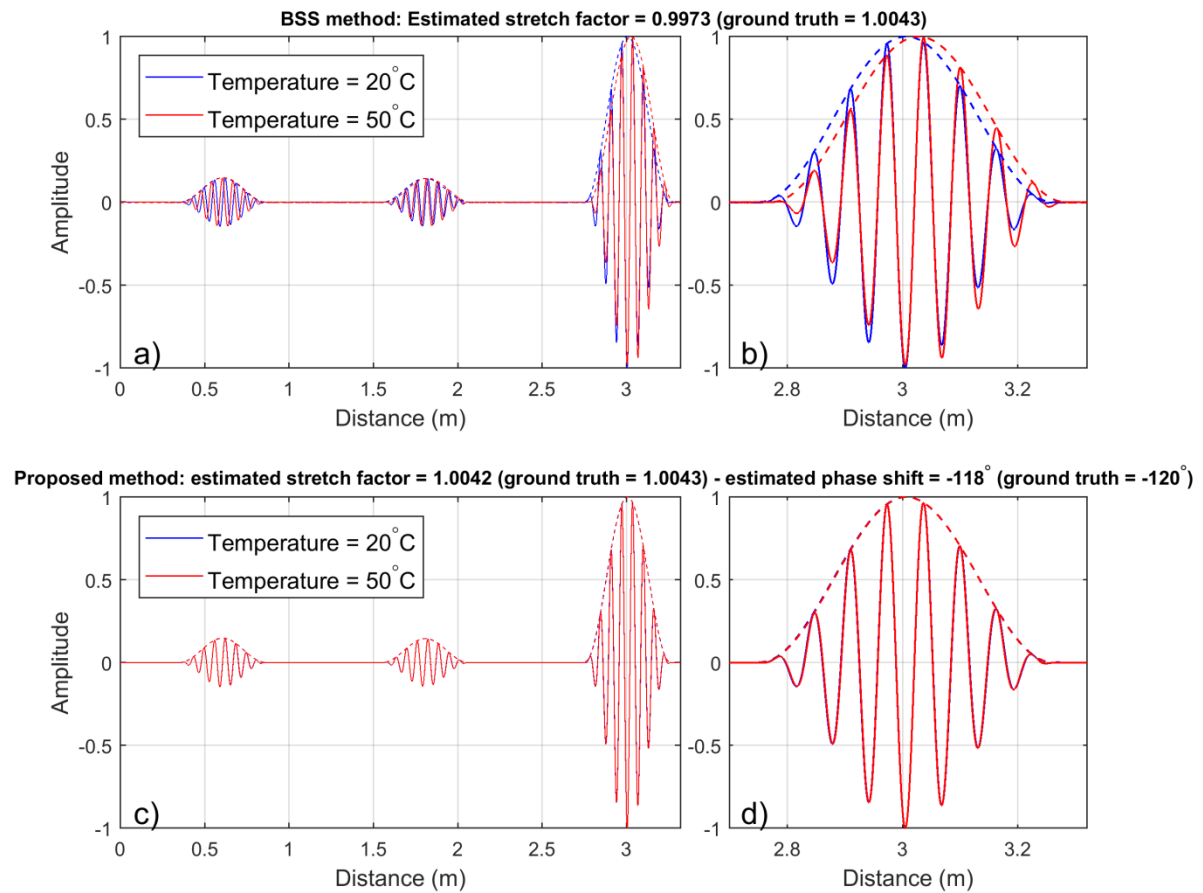
5

Figure 3. a-b) Signals of Figure 2 after temperature compensation using the standard baseline signal stretch method ((b) Zoom on the reflections from the end of the pipe). c-d) Signals of Figure 2 after temperature compensation using the proposed method ((d) Zoom on the reflections from the end of the pipe).

If the phase shift between the tonebursts transmitted in the baseline signal and in the signal to be compensated (the 'current' signal) were known in advance (as is the case for the simulations presented here), an easy solution to improve the efficacy of the BSS technique would be to modify the phase of the current signal prior to the application of the BSS algorithm. Unfortunately, in typical experimental settings, the underlying phase shift between the baseline and the current signal is unknown. For this reason, the method presented here seeks to minimize the residuals by varying both the stretch factor and the phase of the current signal. The range of possible phase shifts can be discretized in steps of, for instance, 1° (i.e. 1°, 2°, 3°,…, 360°), and for each phase shift applied to the current signal a stretch factor corresponding to the minimum value of normalized squared error (NSE) of residuals is computed using the standard BSS technique [13]. Finally, the phase shift and stretch factor associated with the minimum NSE value across the whole range of applied phase shifts and stretch factors are assumed to be good estimates of the actual phase shift and temperature-compensating stretch factor. Clearly, more efficient algorithms can be designed to search for stretch factor and phase shift minimizing the

6

residuals rather than looping through each possible phase shift value, as discussed later. Figure 4 shows the output of this proposed procedure applied to the two signals plotted in Figure 2. The minimum value of NSE of the residuals is obtained when applying a phase shift $\hat{\varphi} = 242°$ to the signal at 50 °C, which is a good estimate of the "true" phase shift $\bar{\varphi} = 240°$ (equivalent to $\bar{\varphi} = -120°$). This estimated phase shift leads to a stretch factor of ~1.0042, virtually identical to the ratio between the wave speeds at the two temperatures (~1.0043). The resulting temperature-compensated signals are plotted in Figure 3(c-d). It should be noted that in this case both the RF signals and corresponding envelopes are well aligned, due to the correct estimation of the stretch factor.
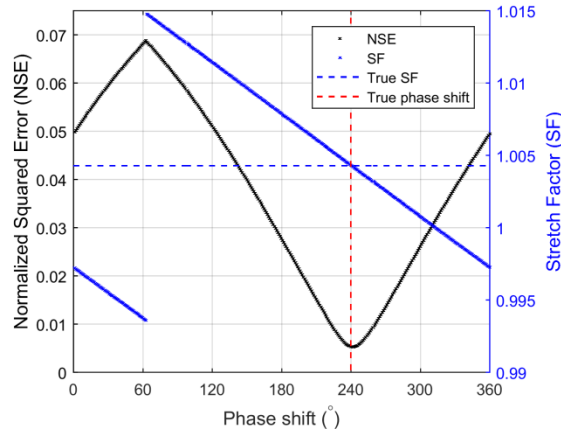

Figure 4. Output of the proposed method applied to the signals of Figure 2: normalized squared error (NSE) of residuals and estimated stretch factor (SF) as a function of phase shift applied to the 'current' signal at 50 °C.

To demonstrate the potential benefit of using the proposed method for defect detection purposes, a signal that simulates the reflection expected from a defect with uniform frequency response [24] (i.e. so the shape of the reflected signal is the same as that of the input signal) located at 0.72 m and with a peak amplitude of 5 % of the pipe end reflection, was synthetically added to the 50 °C signal of Figure 2. This was done by superposition following a procedure proposed by Liu et al. [25] and validated by Heinlein et al.[26]. The defect signal, the resulting 'damaged' signal at 50 °C and the 'undamaged' signal at 20 °C are all plotted in Figure 5. Because the simulated defect is only 120 mm beyond the first weld, which is less than the length of the input wave packet, the weld and defect reflections partially overlap, producing the distorted reflection seen in the figure. Finally, Figure 6 shows the residuals obtained when using the standard BSS method and the proposed method on the defect-free signals of Figure 2 and in the case of Figure 5, where a defect is present in the 50 °C signal but not in the 20 °C baseline. The residuals obtained when using the standard BSS technique are characterized by large values at the locations of the benign features (the two welds and the end of the pipe), both when the pipe is in the undamaged state (Figure 6(a), obtained by subtracting the two signals shown in Figure 3(a)) and when it includes the defect signature (Figure 6(b)). Therefore, in this case it would not be trivial to detect the defect without also suggesting there were defects at the other features. When instead the proposed temperature compensation method is applied to the undamaged signals, the resulting

7

residuals due to the benign features are small and mostly due to the so-called frequency distortion noise [27], as seen in Figure 6(c), which was obtained by subtracting the two signals shown in Figure 3(c). Therefore, it will be easier to detect a new reflection component caused by a structural change, even if it overlaps the reflections from benign features. This is illustrated in Figure 6(d) where the 5% defect reflection just after the first weld is correctly identified. The residual at the pipe end location is similar to that in the absence of a defect (Figure 6(c)). It should be noted that the superposition procedure used to insert the defect signal ignores the small change in the signal transmitted past the defect and so ignores the small changes in subsequent reflections from features.
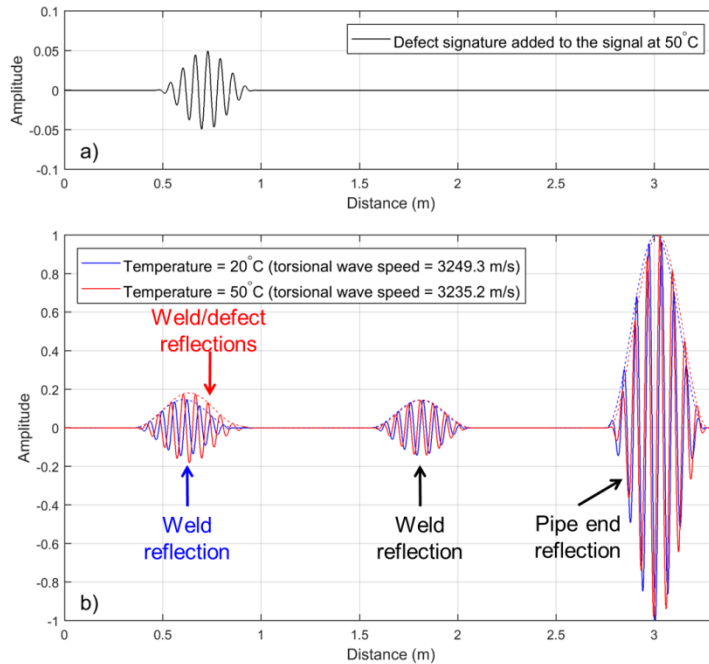

Figure 5. a) Signal simulating the reflection from a point defect located at 0.72 m. b) Simulated torsional guided wave signals traveling in the "forward" direction of the modeled pipe of Figure 1, with the addition of the defect signature shown in (a) being synthetically added by superposition to the undamaged signal at 50 °C. Distances are measured from the center of the transmitted toneburst.
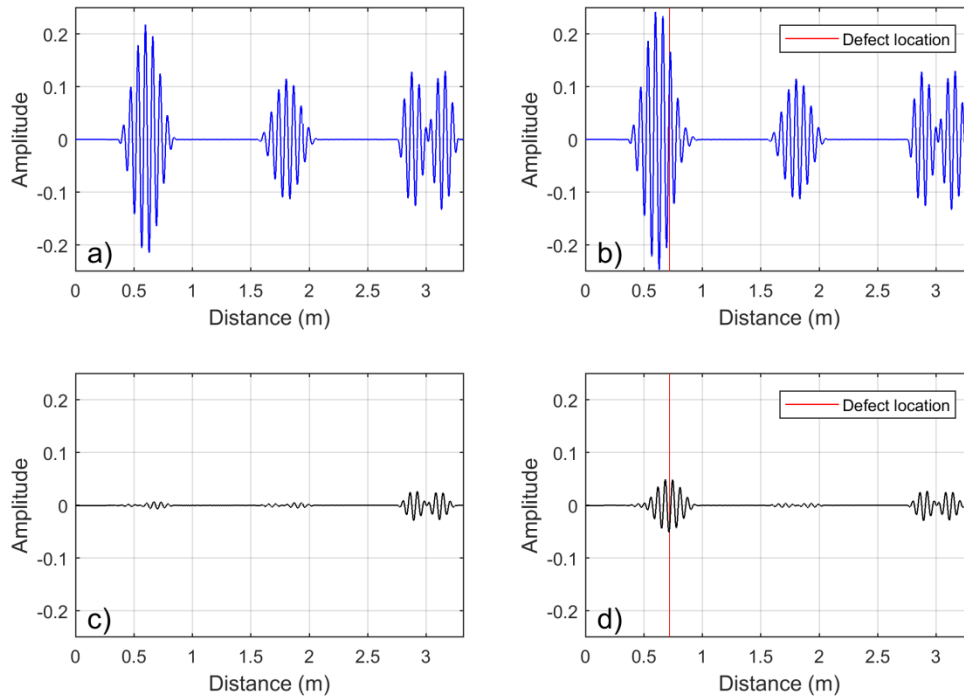
Figure 6. Comparison of the residuals obtained when using the BSS method ((a) undamaged pipe, (b) pipe with simulated defect at 50 °C) and the proposed method ((c) undamaged pipe, (d) pipe with simulated defect at 50 °C).

Application to experimental data

The temperature compensation method illustrated in the previous section was tested on a dataset of torsional ultrasonic guided wave signals acquired by a Guided Ultrasonics Ltd gPIMS® sensor ring [28] attached to an 8 inch schedule 40 pipe in a temperature controlled laboratory setting [29]. As shown in Figure 7, the pipe comprised a 7 meter straight section with a 90° elbow (with a bend radius of 1.5 times the outer diameter of the pipe itself) and a further 2 meter straight section after the bend, and the sensor was installed 4.5 m from the left hand end. In addition to the elbow welds, there was a girth weld in the longer straight section of the pipe. The measurements used to perform the analysis reported in this section pertain to the 'forward' direction indicated in Figure 7, and were acquired prior to the introduction of any defect reported in [29]. Figure 8(a) shows the temperature that was measured by a sensor installed on the pipe near the sensor ring while the measurements were collected, while Figure 8(b) shows signal # 1, which was acquired at 19.1 °C and which was used in this study as the baseline when applying either the BSS or the proposed temperature compensation method to every other signal in the dataset.
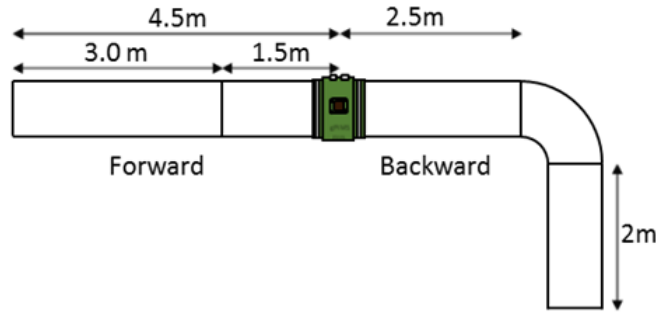
Figure 7. Dimensions of the inspected pipe. The direction considered for this analysis is the "forward" direction.
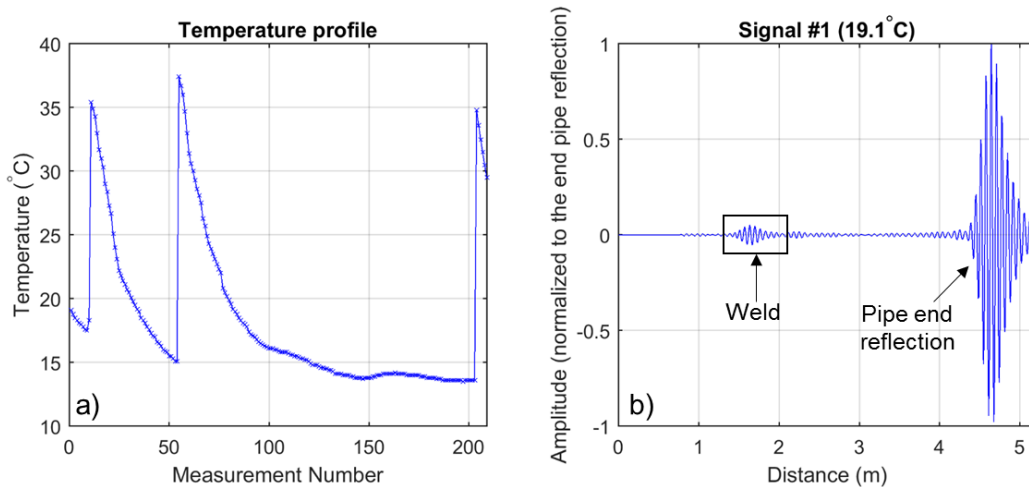

Figure 8. a) Pipe temperature as measured by a sensor placed near the gPIMS® sensor ring. b) Measurement # 1 that was acquired at 19.1 °C and was used as the baseline signal.

Because actual sensor systems can suffer from jitter and therefore may not switch from transmit mode to record mode at exactly the same time on all occasions, one recorded signal might be delayed by a time delay τ relative to another [27,30]. For this reason, the proposed temperature compensation method was enhanced by allowing the search for the minimum NSE of residuals to include the possibility to apply a time delay to each current signal, in addition to a phase shift and a stretch factor. To reduce computational time, this enhanced method was implemented by using a genetic algorithm optimization solver [31].

Figure 9 shows both the baseline signal and the temperature-compensated signal # 55, which was acquired at the highest temperature, namely 37.4 °C, when using either the standard BSS method or the proposed method; the plots are zoomed at the reflections from the weld. Figure 9(b) shows that the proposed method produces a modified current signal that better matches both the RF peaks and envelopes of the baseline signal, when compared to the outcome of the BSS method shown in Figure 9(a), in a similar fashion to that achieved with the simulated signals of the previous section (Figure 3). However, the match between the signals in Figure 9(b) is not perfect; this is likely to be partly due to the application of a constant phase shift across the

10

frequency range of the current signal, whereas in practice the phase shift of the input signal due to a change in temperature is likely to be frequency dependent [9,16].
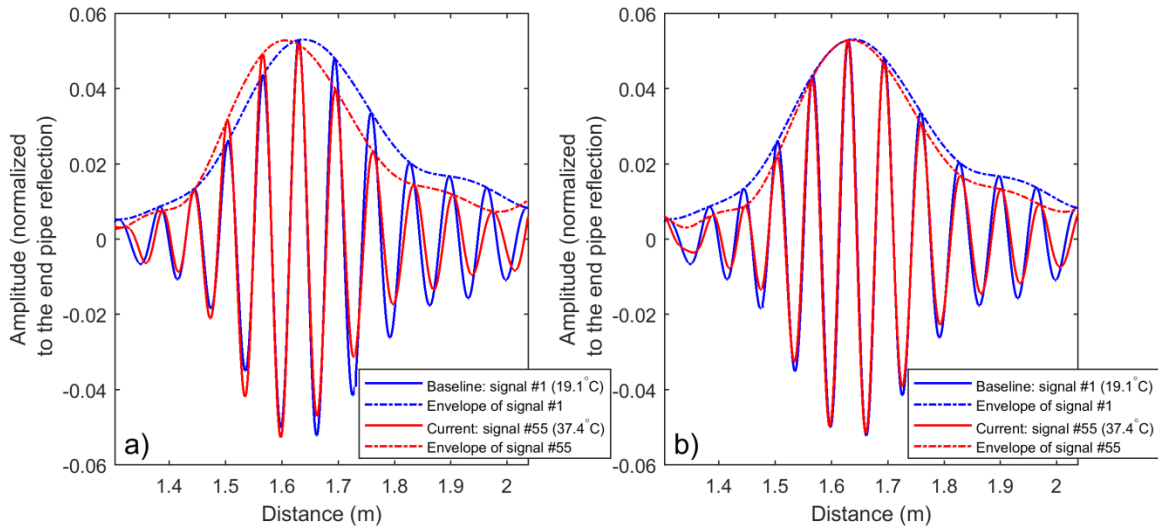

Figure 9. Temperature-compensated signal # 55 and unmodified baseline signal # 1 (roughly 18 °C temperature difference between the two) when using (a) the BSS method; (b) the proposed method. The plots are zoomed to show the reflection from the weld in the forward direction of Figure 7.

Figure 10(a) shows the NSE of the residuals obtained when using the two techniques on each of the 208 measurements at different temperatures of Figure 8(a), always using signal # 1 as the baseline signal. When the temperature at which the 'current' signal is collected is close to that of the 19.1 °C baseline, the NSE approaches zero with both the BSS and the proposed methods, as would be expected since little compensation is required. However, the error obtained with the BSS method increases rapidly as the temperature difference increases, while the proposed method gives a better result. For example, when the 'current' signal is collected at 35 °C the NSE with the proposed method is half that with the standard technique and the fractional improvement is larger at higher temperature differences. Figure 10(b) plots the estimated phase shift between the baseline signal and the different 'current' signals as returned by the proposed method. At least within the range of temperatures of this laboratory trial, the estimated phase shift monotonically increases as the temperature difference between the current and baseline signals increases, and, conversely, monotonically decreases for temperatures lower than that at which the baseline signal was acquired.
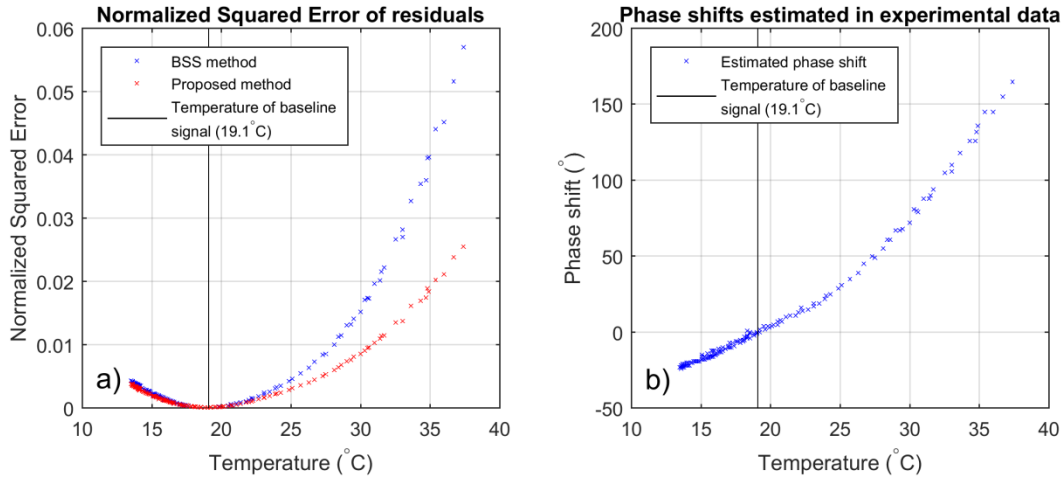
11

Figure 10. a) Comparison of the normalized squared error of residuals obtained when using either the standard BSS method (blue) or the proposed method (red), plotted as a function of temperature. (b) Estimated phase shift existing between each measurement and the baseline signal.

Predicted defect detection performance

Procedure used to generate synthetic coherent noise

FE simulations can be used to predict guided wave propagation in pipes of different geometries and featuring benign features and defects as desired. However, especially when the goal is to estimate the expected defect detection performance under different testing conditions, it is crucial to set up the analyses in a way to include noise with similar characteristics to that seen in actual experimental testing. One difficulty faced by manufacturers of either piezoelectric or EMAT based sensor rings for pipes is to ensure that each transducer employed in the ring has the same transfer function; however in practice it is virtually impossible to achieve identical behavior. For example, when using piezoelectric transducers, one important source of variability is the coupling at the interface between each transducer and the structure. Unavoidable small differences in the adhesive bonded or dry-coupled stiffness will result in a non-uniform distribution of wave amplitudes excited by each transducer, and this variation will be temperature sensitive. With EMATs, circumferential variation of the permeability of the pipe [32,33] will affect the transduction sensitivity. Also, when the temperature changes, it is likely that the distribution will vary due to impedance changes with temperature [16]. This non-uniform distribution of transduction sensitivity is responsible for the generation and reception of unwanted flexural and circumferential modes.

In order to replicate these effects, in each simulation reported in this and subsequent sections, different input signals were assigned to each transducer in the FE model. While the shape of each input signal was a Hanning-windowed 8 cycle sinusoid centered at 25.5 kHz, the peak amplitude of the envelope was set to a random value bounded between 0.5 and 1.5. The same values were also used to weight the individual received signals before they were summed to give the signal

12

corresponding to the T(0,1) mode [22,23]. The procedure is illustrated in Figure 12 that shows a 26 transducer ring with two different random distributions of transducer sensitivities, 'case 2' and 'case 3'. For comparison, the case of the desired uniform distribution of wave amplitudes is also shown as 'case 1'. FE simulations were performed for each of the three cases for a feature-free 7 m long 8 inch schedule 40 pipe, with the sensor ring installed 3 m away from the closest end of the pipe (as shown in Figure 11), and for a simulated temperature of 20 °C. The resulting signals are shown in Figure 13. While 'Case 1' shows virtually zero coherent noise level throughout the whole time trace, the signals from the other two cases show amplitudes up to about 0.6% of the pipe end reflection to which the amplitude is normalized. The coherent noise seen in these conditions is essentially due to circumferential A0 and S0-like modes [34], at least for the first part of the signal, which is before any flexural modes can reach the sensor after being reflected by the end of the modeled pipe.
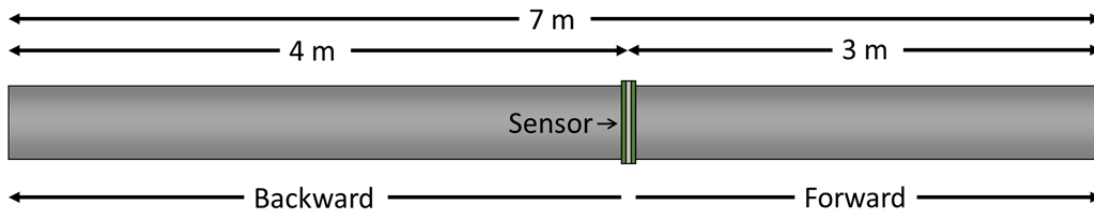

Figure 11. Dimensions of the modeled 8 inch schedule 40 pipe used in the analysis of section "Procedure used to generate synthetic coherent noise"
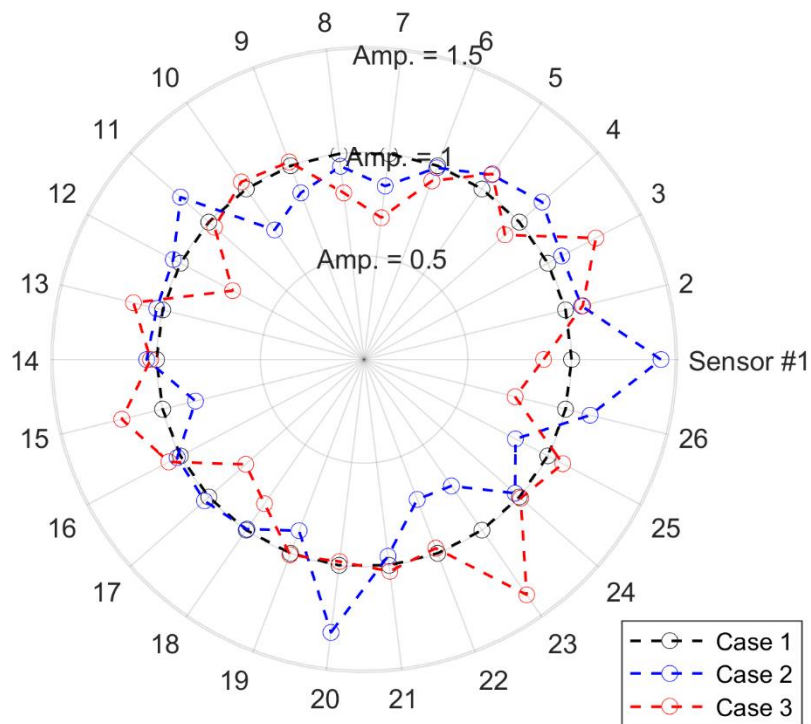

Figure 12. Peak amplitude of the toneburst generated by each simulated transducer deployed around the pipe external circumference. The same values are also used to weight the displacement histories experienced by the same nodes. Comparison between the case of the desired uniform amplitudes (case 1) and two possible cases of non-uniform ones (cases 2 and 3).
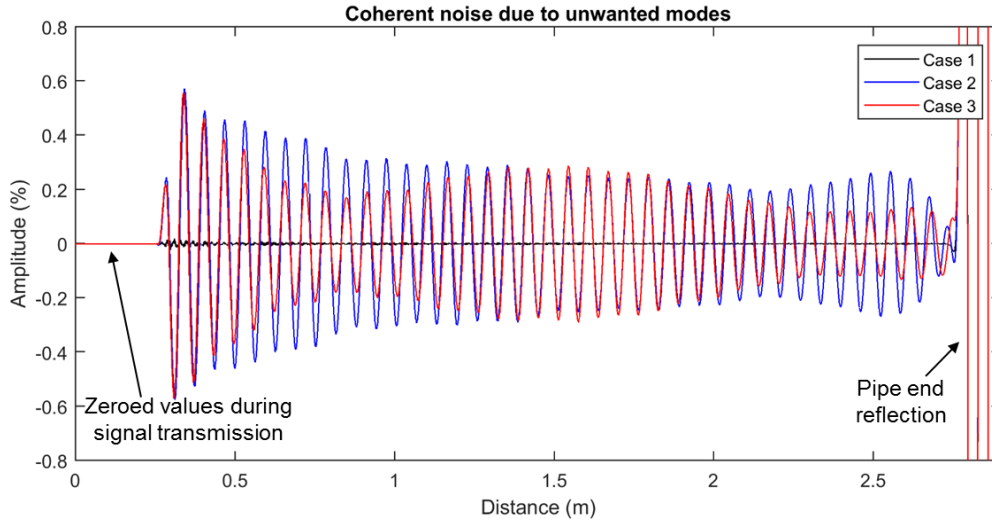
Figure 13. Predicted coherent noise for the transduction rings of Figure 12; the amplitude is normalized to the pipe end reflection. The pipe end reflection approaches 100% and so is severely clipped.

Parameters used to generate synthetic datasets and to compute ROC curves

ROC curves were first introduced in statistics to illustrate the performance of a binary classifier [20]. In recent years, ROC curves have become increasingly popular in the field of NDE/SHM as a tool to assess the defect detection performance achievable by a detector system set to operate at different operational conditions [25,35,36]. These curves plot the probability of detection (POD) of a given defect size versus the probability of false alarm (PFA) at various threshold values.

In this study, a large dataset of synthetic signals at different temperatures was created, which was then used as a basis to compute ROC curves. The signals simulated the testing at various temperatures (ranging from 20 to 75 °C) of the forward direction of the pipe shown in Figure 11 with a 1.8 m test range from the transducer ring with the addition of a weld and, for some of the signals, a defect, both of them placed at various positions within the test range and having different sizes, depending on the particular case. Details on the parameters used to model the effects of temperature are given in Table 1. Figure 14 gives an overview of the overall structure of the dataset. The two scenarios differ in the phase assigned to the input signal: in "scenario 1" it was kept constant throughout the whole temperature range, while in "scenario 2" it was varied with temperature, thus obtaining a more realistic dataset. Each scenario comprised 120 batches of synthetic signals, whereby each batch was formed by 50 different realizations of simulated testing, at the various temperatures, of the pipe featuring one specific weld and, in the defective cases, one specific defect. The test parameters used to simulate the different batches are given in Table 2. Each batch was generated using one value for each parameter. For example, in one batch the simulated pipe included a weld at a distance of 0.65 m from the sensor, whose reflection coefficient was 10 dB above the noise level, and, for the signals including the defect, it was inserted 1.21 m from the sensor with a peak amplitude 6 dB above the noise floor. The

14

different realizations were obtained by superposing the desired pipe features on different FE-generated coherent noise time traces. For each scenario and for each considered temperature, 50 FE simulations were run on the feature-free modeled pipe of Figure 11 following the procedure illustrated in the previous section, thus obtaining a large set of randomly generated coherent noise time traces. This equated to a total of 900 simulations to run ("cases 2 and 3" shown in Figure 12 and Figure 13 are two of the outcomes at 20 °C in the 2nd scenario). Because pipes used in the field do not have open ends from which the guided wave signal would be entirely reflected (unlike pipes installed in laboratory settings), it was decided not to include the pipe end reflection on the signals to be analyzed. Considering this, and also driven by the need to reduce the total computational time and the volume of data to handle, the simulations were run for the duration needed for the torsional waves to cover a return trip of 1.8 m from the sensor ring, as already mentioned. The arrival time of each weld and damage synthetic reflection was computed by using the T(0,1) wave speed, listed in Table 1; this ensured that each reflection was inserted at the same spatial location in each signal obtained at different temperatures. Signals containing only a weld reflection (pristine) and with both weld and defect reflections (defective) were produced at each temperature apart from 20 °C where only pristine signals were generated to use as baselines.
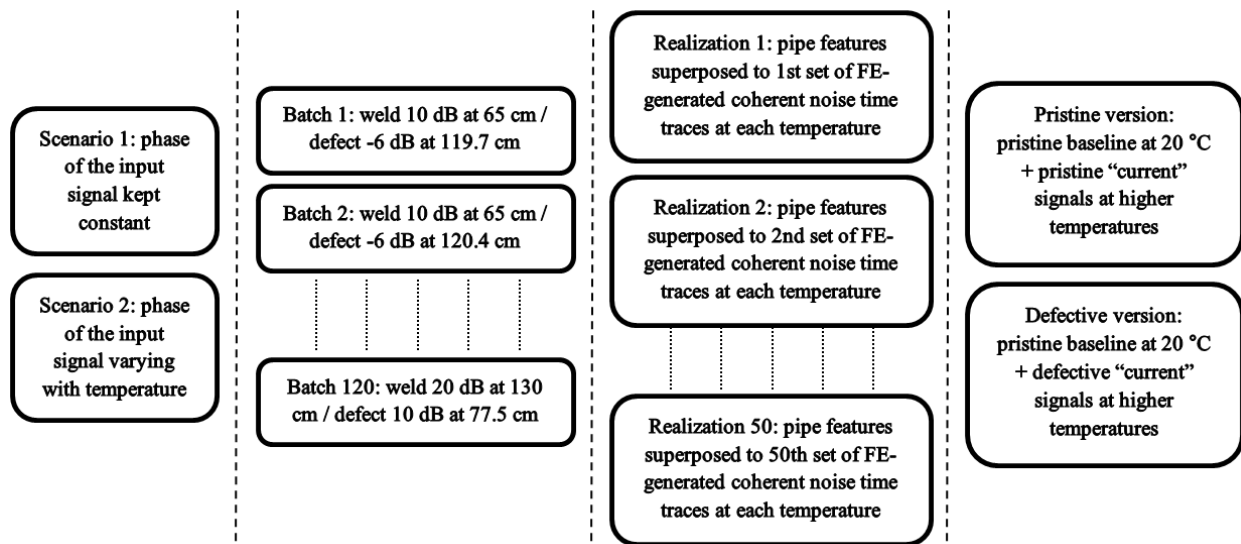

Figure 14. Schematic of the generated synthetic datasets. Each of scenarios 1 and 2 included 120 batches of data, each batch comprising 50 realizations of testing both a pristine and a defective version of the same pipe at various temperatures. Specifically, each batch corresponds to a specific set of modeled pipe features, as listed in Table 2, and each realization is characterized by having different FE-simulated coherent noise time traces. For each realization, both a "pristine" and a "defective" version was formed, whereby the baseline signal at 20 °C was always pristine, while the signals at higher temperatures either did not include the defect signature (pristine) or did include it (defective).

Table 1. Parameters used to model the effects of the different temperatures.

Temperature (°C)	20	27	34	41	48	55	61	68	75
T(0,1) wave speed (m/s)	3249.3	3246.0	3242.7	3239.4	3236.1	3232.9	3230.1	3226.8	3223.5
Phase of input toneburst (°) (only for "scenario II")	90	62	34	6	-22	-50	-74	-102	-130

Table 2. Test parameters used to generate synthetic signals including a weld and a defect.

Parameter	Value	Unit
Weld amplitude (wrt noise level)	10, 20	dB
Defect amplitude (wrt noise level)	-6, 0, 3, 6, 10	dB
Weld location	65 (#1), 130 (#2)	cm
Defect location (for weld location #1)	119.7, 120.4, 121, 121.7, 122.3, 123	cm
Defect location (for weld location #2)	74.3, 74.9, 75.6, 76.2, 76.9, 77.5	cm

Figure 15 shows how each synthetic signal was built up using the case of the pristine record at 20 °C featuring the weld at 0.65 m and at 20 dB wrt noise level being superposed on the coherent noise time trace obtained using the simulated sensor of "case 2" in Figure 12, as an example. Firstly, each coherent noise time trace obtained from each FE analysis was compensated to remove the amplitude decay with distance seen in Figure 13. In practice the coherent noise can decay with distance if it is largely due to circumferential modes or can be constant or increase as reflections of flexural modes from features build up. Keeping it constant is reasonably representative and facilitates easy comparison of ROC curves for defects of a given size at different locations. The amplitude compensation was achieved by multiplying the original predicted time trace of Figure 15(a) by the exponential function of Figure 15(b) to give the trace of Figure 15(c) which was normalized by the average value of its envelope (without taking into account the values of the first 0.3 m). The unit normalization value gave the reference amplitude when inserting either a synthetic weld or a synthetic defect at the desired signal to noise ratio (SNR). For instance, Figure 15(d-e) shows the superposition of a synthetic weld signature with a SNR of 20 dB. Where needed, the defect signatures were added in the same fashion. For simplicity, both the welds and defects considered throughout the dataset were modeled as reflectors with zero-axial length and uniform frequency response. Finally, each resulting time trace was normalized to unity at the peak of its envelope.
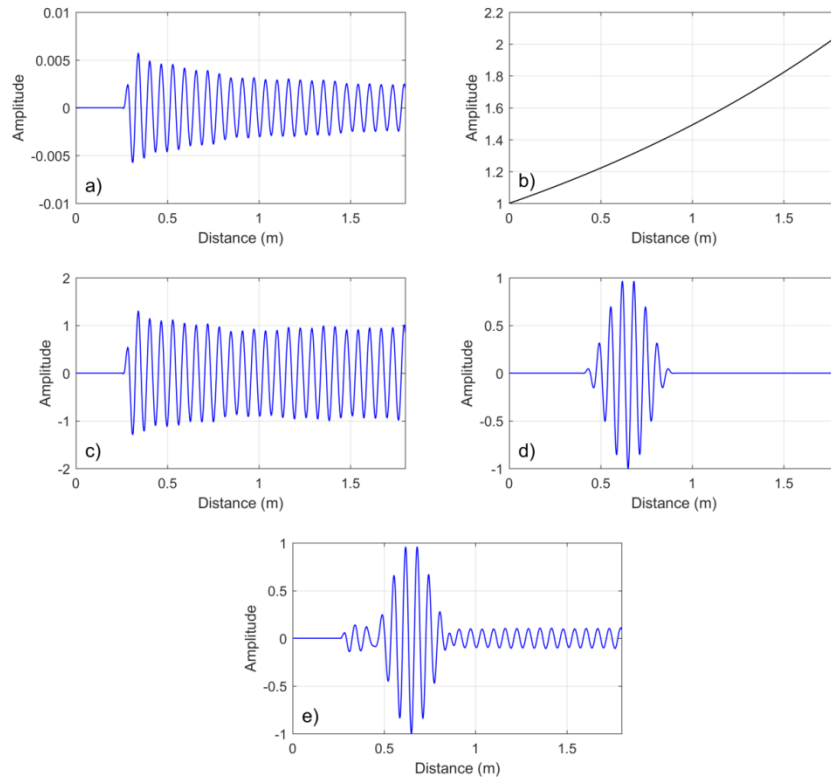
Figure 15. Procedure used to generate a synthetic signal at 20° C featuring a weld 20 dB above the noise floor. a) Coherent noise time trace (same as the initial 1.8 m of "case 2" in Figure 13). b) Exponential function applied to the time trace in order to balance the decaying amplitude. c) Resulting un-decayed time trace, normalized by the average value of its envelope (not taking into account the first 0.3 m). d) Synthetic weld signature (of zero-length and uniform frequency response). e) Synthetic signal obtained by superposing the weld signature at the appropriately scaled coherent noise time trace.

Once the dataset was formed, each individual signal at a temperature higher than 20 °C was processed by using the baseline subtraction technique with respect to the baseline signal at 20 °C from the same set of realizations (e.g. the "current" signals in the set of realizations #1 were compared to the baseline obtained in the same set) using each of: no temperature compensation method (in the following this will be denoted "method 1"), the standard BSS method ("method 2") or the method presented in this paper ("method 3"). However, in the 1st scenario, where the phase of the input signal was not varied with temperature, only "methods 1 and 2" were used. For example, Figure 16 shows the temperature-compensated defective signal at 27 °C obtained in the 2nd scenario in the 1st realization of the simulated pipe including a weld and a defect 20 and 6 dB above the noise level and 0.65 and 1.21 m away from the sensor, respectively. For method 1 (Figure 16(a,d)), the current signal was directly subtracted from the baseline signal to produce the residuals displayed in Figure 16(d). The magenta trace in the same figure is the envelope of the synthetic defect signature that was added to the 27 °C signal, thus representing the optimal outcome of the baseline subtraction. While the residuals obtained with this method correctly show the defect component, a stronger component due to the imperfect alignment of the weld

17

reflections is also present. By using method 2, as seen in Figure 16(b,e), the improved alignment of the weld reflections produces residual components at the weld smaller than the ones at the defect. A similar outcome is also obtained with method 3, as shown in Figure 16(c,f). When the temperature difference between current and baseline signals widens to 41 °C, as in Figure 17, which shows the 1st realization of testing the same defective pipe as in Figure 16 but at 61 °C, the results of both methods 1 and 2 are affected by increased residual values at the weld (roughly 5-fold for method 1 and 3-fold for method 2), while the residuals obtained with method 3 and shown in Figure 17(f) remain similar to those seen in Figure 16(f). Both of these figures show the correct defect amplitude and minimal residuals at other locations. Finally, it should be noted that in this case the residuals at the defect obtained by using method 2, shown in Figure 17(e), also increased to amplitudes almost twice as large as the inserted defect component. This is due to the defect signature being out of phase, at the computed stretch factor, with the coherent noise in the baseline signal at the same location. It will be appreciated that if a defect of the same size was placed at a slightly offset position then reduced residuals would be obtained. In order to capture the effect of this varying interference on detectability, multiple defect positions within a half-wavelength distance (namely ~32 mm) were considered when setting up this study, as listed in Table 2.
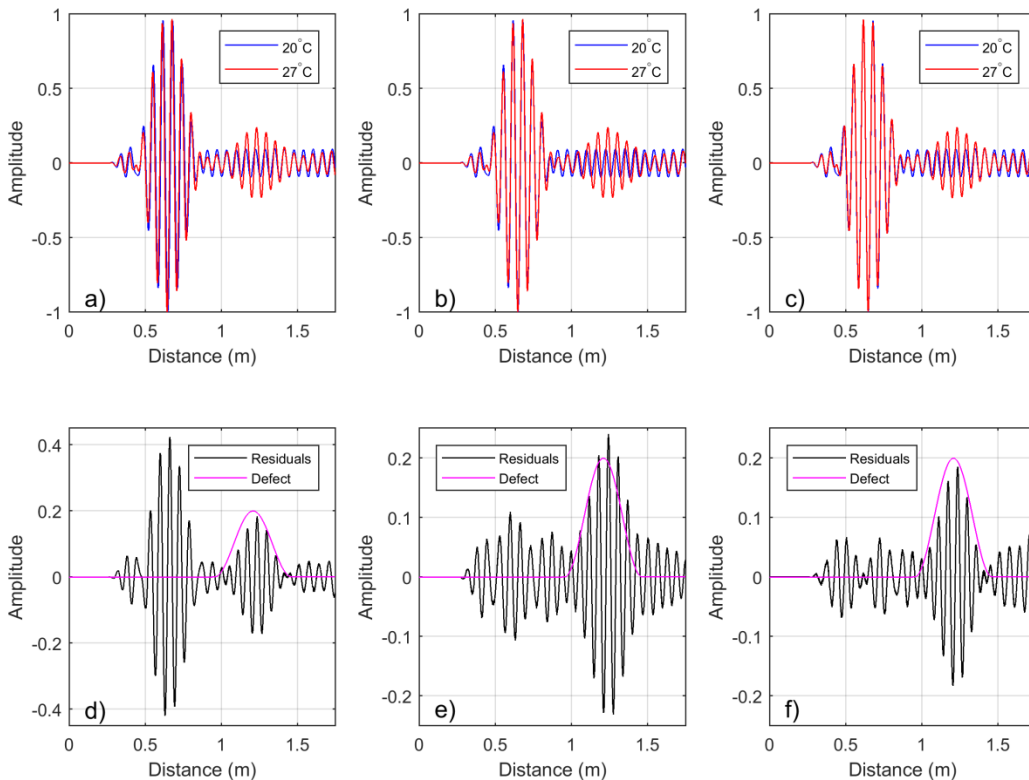

Figure 16. Temperature compensation of a synthetic defective signal obtained at a 7 °C higher temperature than the baseline, in the 2nd scenario. The signal comprises a weld and a defect 20 and 6 dB, respectively, above the noise floor. Results of "method 1": (a) uncompensated 27 °C signal and 20 °C baseline signal; (d) corresponding residuals. Results of "method 2": (b) BSS-compensated 27 °C signal and 20 °C baseline signal; (e) corresponding residuals. Results of "method 3": (c) 27 °C signal after compensation with the proposed method and 20 °C baseline signal; (f) corresponding residuals. The envelope of the synthetic defect added to the 27 °C time trace is shown in magenta in plots (d,e,f).
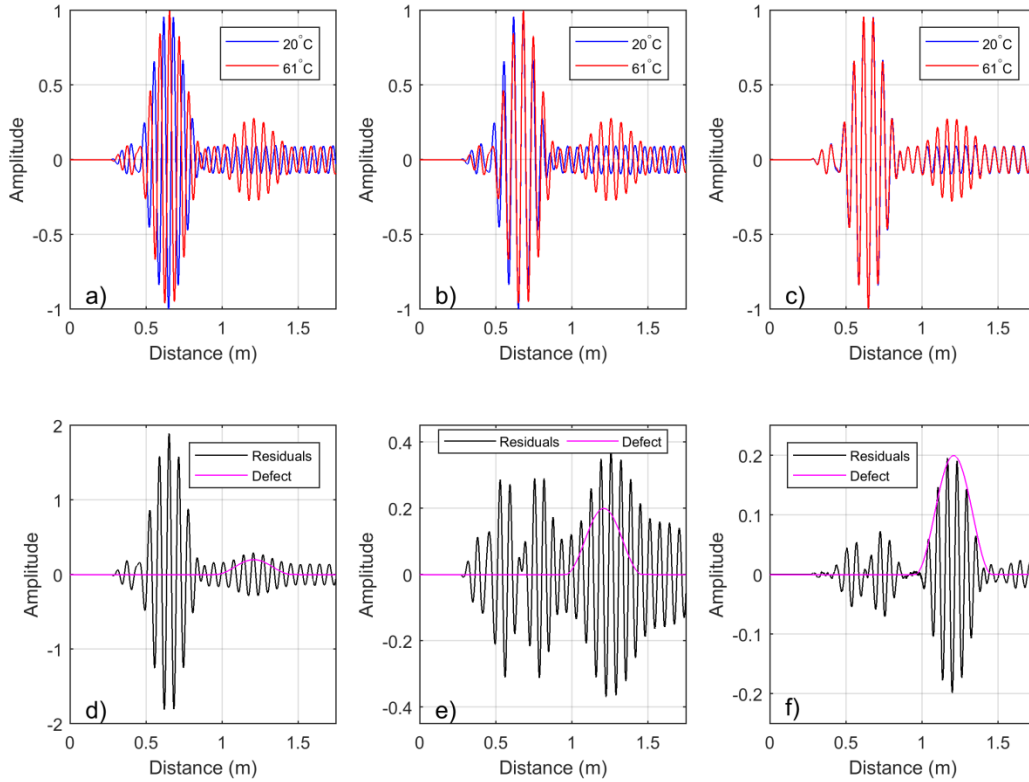
18

Figure 17. Temperature compensation of a synthetic defective signal obtained at a 41 °C higher temperature than the baseline, in the 2nd scenario. The signal comprises a weld and a defect 20 and 6 dB, respectively, above the noise floor. Results of "method 1": (a) uncompensated 61 °C signal and 20 °C baseline signal; (d) corresponding residuals. Results of "method 2": (b) BSS-compensated 61 °C signal and 20 °C baseline signal; (e) corresponding residuals. Results of "method 3": (c) 61 °C signal after compensation with the proposed method and 20 °C baseline signal; (f) corresponding residuals. The envelope of the synthetic defect added to the 61 °C time trace is shown in magenta in plots (d,e,f).

ROC curves are computed by sweeping a threshold value over the range of values in the residual curves of the type shown in Figure 16(d-f) and assessing at each threshold value whether the defect of interest is detected or not and whether there are false calls in the case of no defect being present. This is illustrated in Figure 18 which shows both the defective residual signals shown in Figure 16(d-f) and their corresponding pristine residual signals (i.e. the 1st realization of testing the same pipe as in Figure 16 at 27 °C but with no synthetic defect added). The threshold is swept on the envelope of each residual signal at values ranging from 0 to 2 split into 2000 steps (it should be noted that 2 is the maximum residual value that would be obtained when the peak values of current and baseline signals are completely out of phase). For illustration purposes, in Figure 18 three of the 2000 threshold values are shown, namely 0.05, 0.15 and 0.25. To calculate the PFA, only the pristine residual signals are considered: firstly, for any given threshold value one false alarm is counted for any pristine residual signal whose envelope exceeds the threshold, whether at only one or at multiple locations (e.g. for the pristine residual signal obtained using method 1 and shown in Figure 18(a), the false alarm is flagged for each of the three thresholds shown in figure, whereas for the residuals obtained with method 2 and 3 of Figure 18(c) and (e),

respectively, only the lowest threshold flags the false alarm); the PFA is computed as the ratio between the total number of false alarms and the number of available pristine residual signals (50 were used in this study as discussed earlier). Similarly, to calculate the POD, only the defective signals are considered, and at any given threshold value one true detection is counted for any defective residual signal whose envelope exceeds this value at any location within a finite length of the pipe equal to the length of the synthetic defect signature and centered at the true defect location (e.g. for the defective residual signal obtained using method 1 and shown in Figure 18(b) the true detection is flagged at the two lower threshold values and is not flagged at the highest one; the same outcome is obtained for methods 2 and 3, shown in Figure 18(d-f)). The POD is then computed as the ratio between the total number of true detections and the number of available defective residual signals (50 in this study). The POD and the PFA calculated at each threshold correspond to one point on the ROC curve, and the collection of the 2000 points from the different threshold values becomes the ROC curve for the particular defect size.
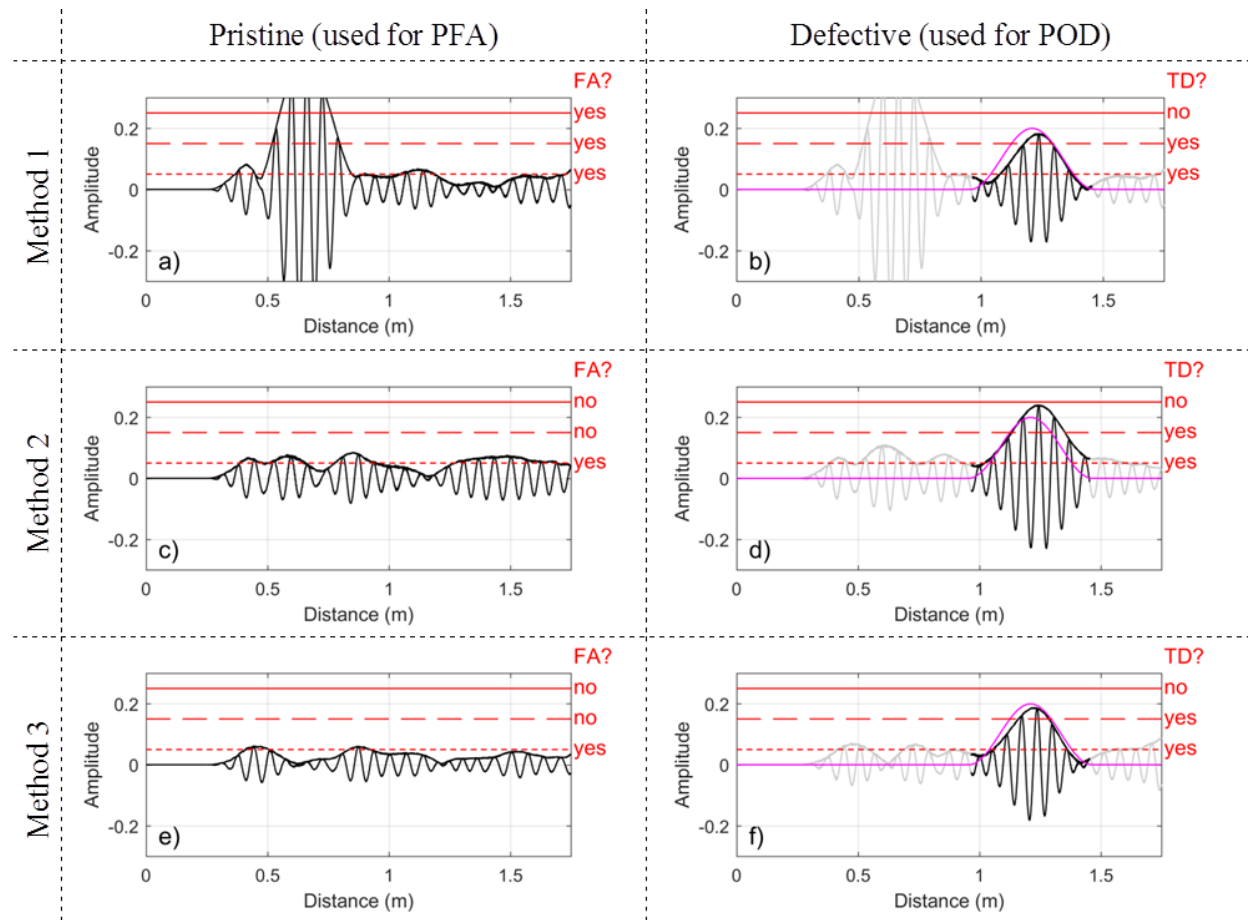

Figure 18. Procedure used to compute the PFA and the POD based on the envelopes of the residual signals. a,c,e) pristine residuals and their envelopes obtained from the 1st realization of testing at 27 °C the same pipe as in Figure 16 but with no synthetic defect added, and using each of the three temperature compensation methods. These are the signals considered to compute the PFA. b,d,f) defective residuals and their envelopes obtained from the 1st realization of testing at 27 °C the same pipe as in Figure 16 and using each of the three methods. The portions of the signals spatially located within a finite length of the pipe equal to the length of the synthetic defect signature and centered at the true defect location (black portions of the signals) are those considered to compute the POD. The envelope of the synthetic defect added to the time trace is shown in magenta. a-f) The

Results from "scenario 1" (constant phase)

As previously stated, only methods 1 and 2 were applied to the synthetic signals pertaining to the 1st scenario, and the salient results from the analysis are presented in this section. Figure 19 summarizes the statistics of the maximum values of the residuals obtained from all the signals with the synthetic weld at 10 dB above the noise level; the upper plot refers to method 1 and the lower plot to method 2. Each plot comprises six frames, each of which shows eight box plots of maximum values of residuals corresponding to different temperature differences from the baseline (e.g. $\Delta T = 7, 14, 21$ °C, …), where the box, the horizontal line and the whiskers indicate, respectively, the interquartile, the median, and the 90% two-sided interval of the values. The leftmost frame refers to the pristine residual signals, where the maximum value of each signal is sought anywhere in the signal itself, as shown in Figure 18(a,c,e); clearly, this is likely to occur at the weld, especially when using method 1, whereby the arrival times of the weld reflection would be increasingly offset as the temperature difference between the current and baseline signals increases. The other five frames refer to the defective signals, where each frame corresponds to a different defect size. As shown in Figure 18(b,d,f), for each of these signals the maximum value is sought within a finite length of the pipe equal to the length of the synthetic defect signature and centered at the true defect location. Because the interest in this case is to analyze to what extent the residuals at the defect are able to indicate the correct defect size, each of these frames also shows the true defect size using a red line.

The results from method 1 are shown in Figure 19(a); for the pristine signals, as the temperature difference ΔT increases, the median values of the residuals increases (as do the interquartile ranges); in contrast, for the defective signals, the median values for the majority of the defect sizes decrease with increasing ΔT (while the interquartile ranges increase), though the values remain fairly close to the true defect sizes. However, as the temperature difference increases, the spread of residuals in the pristine case increasingly overlaps the residuals produced by a defect, and would cause a large number of false calls if the 'call threshold' was set to ensure a reasonable probability of detection. It should be noted that in almost all cases, the highest residuals in the pristine case are at the weld location so the false calls would be at the weld. In contrast, with method 2, the residuals in the absence of a defect do not increase significantly with temperature difference, as seen in Figure 19(b), so the false call rate would not increase as markedly with temperature difference.

Figure 20 plots ROC curves obtained from three interesting cases among the ones shown in Figure 19, namely for defects -6, 0 and 6 dB above the noise level. In each plot the curves corresponding to methods 1 and 2 are shown in black and in red lines, respectively. Also, the eight cases of temperature difference from the baseline are assembled in two groups, the first group comprising ΔTs ranging from 7 to 28 °C (whose results are plotted as solid lines), and the

21

second from 35 to 55 °C (whose results are plotted as dashed lines). The ROC curves are plotted on a semi-log scale as in most monitoring applications, false alarm rates of 1% or below would be required. As already expected from the results shown in Figure 19, when the defect reflection is roughly twice as large as the noise level, as in Figure 20(c), method 2 guarantees virtually perfect detection performance, even at the highest ΔT values. In contrast, when a temperature compensation technique is not used, the predicted detection performance worsens and degrades greatly with the temperature difference from the baseline, as shown by the two black curves corresponding to method 1. This is a direct consequence of the increasing residuals at increasing ΔT for pristine signals shown in the leftmost frame of Figure 19(a). When the defect reflection is close to the noise floor, as in the case of Figure 20(b), the performance of method 2 is still much better than method 1 but the false alarm rate at high POD would probably be unacceptable. Finally, Figure 20(a) shows that even using method 2 it would be impossible to target defects giving reflection amplitudes roughly half of the average noise level.
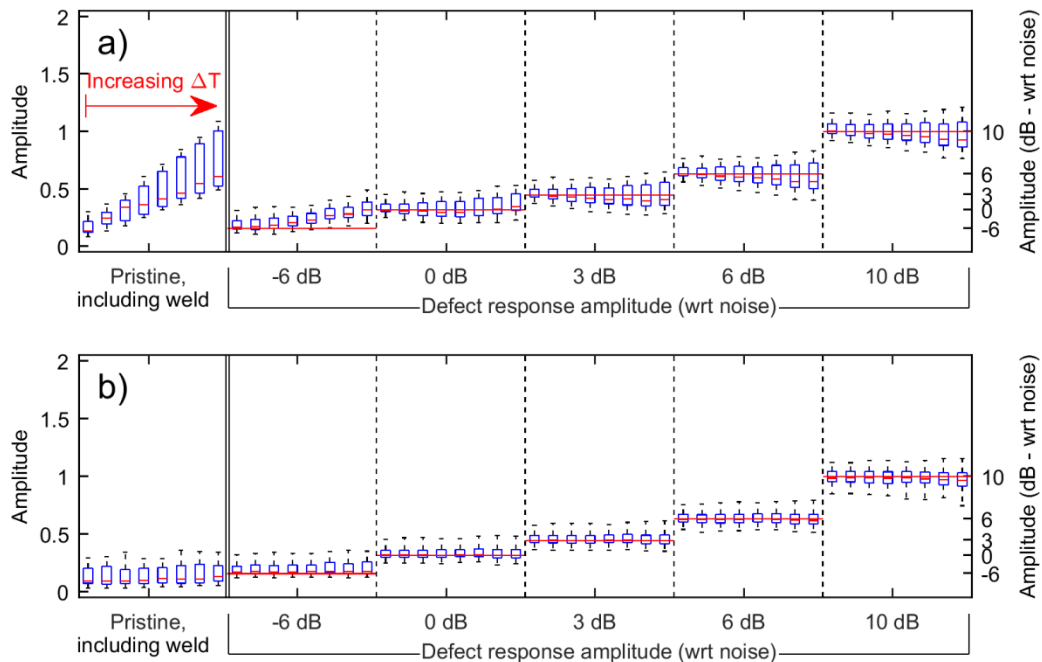

Figure 19. Box plots of the maximum values of residuals obtained from all the signals of scenario 1 with the synthetic weld at 10 dB above the noise level. a) Results from method 1. b) Results from method 2. In each plot, the leftmost frame refers to the pristine residual signals, and the other five frames refer to the defective signals, at increasing defect sizes. The maximum values are sought across each entire signal for the pristine ones, and only around the defect location for the defective signals, as shown in Figure 18. In each frame, the eight box plots correspond to different temperature differences from the baseline (e.g. ΔT = 7, 14, 21 °C, …), and the box, the horizontal line and the whiskers indicate, respectively, the interquartile, the median, and the 90% two-sided interval of the values. The true defect response amplitude is indicated with a red line in each frame referring to defective signals.
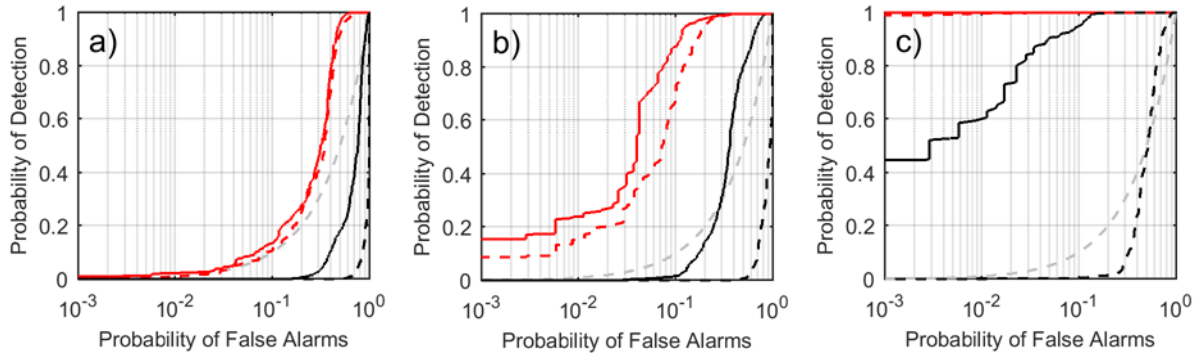
Figure 20. ROC curves computed from the signals of scenario 1 with the synthetic weld at 10 dB above the noise level, and for defects at -6 dB (a), 0 dB (b) and 6 dB (c) above the noise level. The ROC curves from methods 1 and 2 are plotted in black and red lines, respectively. The solid lines refer to signals where the temperature differences from the baseline range from 7 to 28 °C, while the dashed lines have ΔTs ranging from 35 to 55 °C. The light grey dashed line is the random guess performance (which in a linear plot would be a ROC curve following the 45° diagonal line, where the POD and PFA are equal). Note that each plot is on semi-logarithmic scale.

Results from "scenario 2" (phase shifts at different temperatures)

In the 2nd scenario, where the phase of the input signal was shifted with temperature according to the parameters listed in Table 1, each of the three methods was independently applied and evaluated. As in the previous section, only the results from the analysis of the signals with the synthetic weld at 10 dB above the noise level are shown. Analogously to Figure 19, Figure 21 displays the statistics of the maximum values of the residuals obtained when using methods 1, 2 and 3, shown in the upper, middle and lower plots, respectively.

When using method 1 on the pristine signals, as seen in the leftmost frame in Figure 21(a), the resulting residuals increase greatly as the temperature difference ΔT increases, up to values of 2 at the highest ΔT, due to the weld reflections in the current and baseline signals progressively transitioning from being almost in phase to being severely out of phase. Similarly, for the defective signals, the median values increasingly deviate from the true defect sizes as the temperature difference increases, due to the components forming the coherent noise in the two signals also becoming markedly out of phase. By using method 2, whose results are shown in Figure 21(b), the residuals for pristine signals remain at much lower values than with method 1, even though they are still high enough to cause a large number of false calls at likely values of 'call threshold'. In addition, the defect indications in the defective signals are closer to the correct amplitudes than with method 1. Lastly, thanks to the phase correction of method 3, Figure 21(c) shows residuals for pristine signals which remain reasonably low even at the highest temperature difference values; similarly, for the defective cases, the defect sizing is more accurate, and the spread is also reduced, as shown by the interquartile ranges. It should be noted that these results are fairly similar to the ones shown in Figure 19(b) (i.e. by using the proposed method with transducers whose phase response shifts with temperature, it is possible to obtain similar results to those obtained with the standard BSS method for the case of phase stability).

23

Figure 22, analogously to Figure 20, plots ROC curves obtained for defects -6, 0 and 6 dB above the noise level. In this case, the curves corresponding to methods 1, 2 and 3 are shown in black, red and blue lines, respectively. Interestingly, and in line with what can be observed by comparing Figure 19(b) and Figure 21(c), for each of the three defect sizes, the detection performance offered by method 3 in this scenario resembles the one obtained with method 2 in the 1st scenario. Therefore, similar observations apply here, such that defects giving reflection amplitudes twice the size of the noise are detectable by using method 3 with a close to perfect detection performance, at all temperatures. In contrast, when using method 2, the detection performance greatly worsens as the temperature difference ΔT increases, though even for the lowest values of ΔT the false alarm rate at high POD is probably unacceptable. Even worse is the detection performance offered by method 1, where at the highest values of ΔT the dashed black curve is scarcely visible as it virtually coincides with the lower and right borders of the plot (note that the same applies to the same curve in the other two plots of Figure 21). As in the 1st scenario, the detection of defects giving reflection amplitudes at the noise level is possible with high POD only by using method 3 and only by allowing a probably unacceptable false alarm rate, whereas it would be impossible to target defects half of that size. Nevertheless, in both cases, the detection performance of method 3 is again much better than that of method 2, which in turn outperforms method 1.
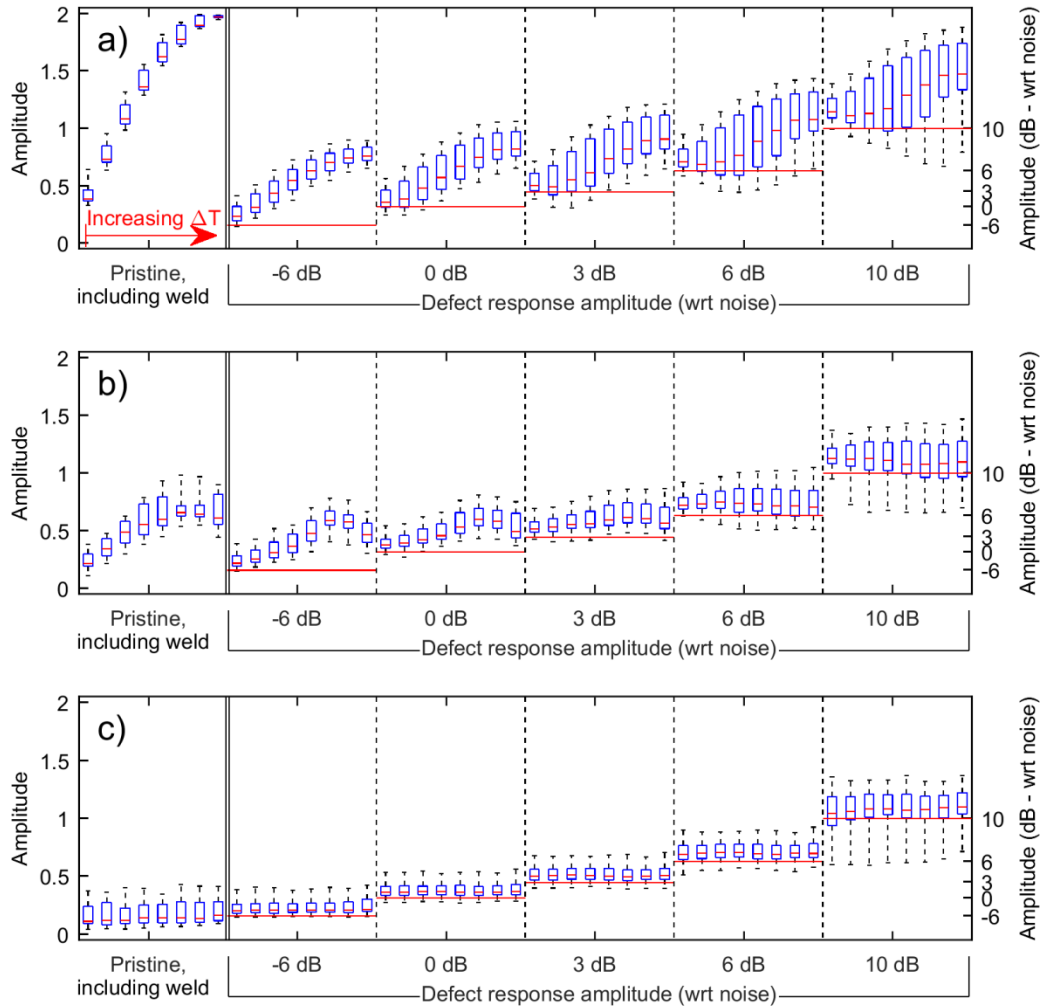
Figure 21. Box plots of the maximum values of residuals obtained from all the signals of scenario 2 with the synthetic weld at 10 dB above the noise level. a) Results from method 1. b) Results from method 2. c) Results from method 3. Symbols and lines used as in Figure 19.
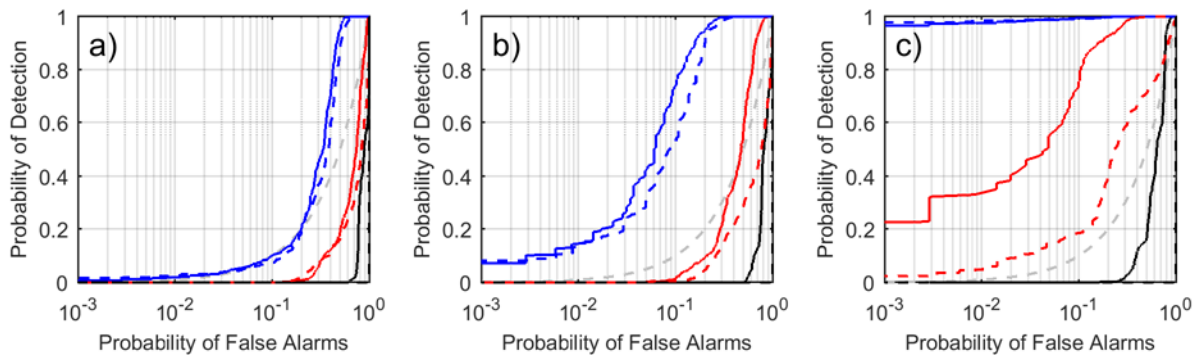

Figure 22. ROC curves computed from the signals of scenario 2 with the synthetic weld at 10 dB above the noise level, and for defects at -6 dB (a), 0 dB (b) and 6 dB (c) above the noise level. The ROC curves from methods 1, 2 and 3 are plotted in black, red and blue lines, respectively. The solid lines refer to signals where the temperature differences from the baseline range from 7 to 28 °C, while the dashed lines have ΔTs ranging from 35 to 55 °C. The light grey dashed line is the random guess performance (which in a linear plot would be a ROC curve following the 45° diagonal line, where the POD and PFA are equal). Note that each

25

plot is on semi-logarithmic scale. Also note that in each plot the black dashed line virtually coincides with the lower and right borders of the plot.

Signals with no benign feature reflections above the coherent noise level

The study presented in the previous sections showed that the stretch compensation methods work well with signals including benign features giving reflections well above the noise level. However, there are cases where the inspected structure either only has features giving reflections lower than the coherent noise, or has no benign features at all over the inspected region. In these cases, there is a concern that in the process of minimizing the difference between the current and baseline signals, the stretch procedure would tend to reduce the size of the defect signal, perhaps to below the coherent noise level, and so reduce the probability of its detection; this issue is examined below.

12 additional batches of synthetic signals similar to the ones described in Figure 14 and Table 2 were generated. These signals featured a very small weld reflection -20dB wrt the noise level and, for the defective cases, a defect 6 dB wrt noise. Both weld and defect were inserted at every location indicated in Table 2 (giving the 12 batches), and both scenarios 1 and 2 were simulated.

The results of this further study are summarized in Figure 23. The upper three plots refer to scenario 1, and the lower three to scenario 2. As seen previously, only methods 1 and 2 were applied to the synthetic signals of the 1st scenario, and Figure 23(a,b) display the statistics of the maximum values of the residuals produced by the two methods, respectively. Each of these plots comprises two frames, the left one referring to the pristine signals and the right one to the defective signals, and is analogous to the ones in Figure 19, although the amplitudes here are normalized to unity at the noise level. Figure 23(d,e) were produced in the same fashion, and refer to the results given by methods 1 and 3, respectively, in the 2nd scenario. Finally, the rightmost plots (Figure 23(c,f)) show the ROC curves obtained from the results seen in Figure 23(a,b,d,e), with the same conventions used to produce Figure 20 and Figure 22. Note that the results with method 2 on the 2nd scenario are not shown for the sake of clarity, but they yielded a worse detection performance than method 3, similarly to what was already seen in Figure 22.

As seen previously, when using a stretch-based compensation method in both the 2nd and 3rd scenarios, the residuals of pristine signals are bounded to lower values than when using method 1, especially at the higher temperature differences. Again, this is clearly beneficial to limit the number of false calls at likely values of 'call threshold'. For the defective signals, the strong variability of the residuals seen with method 1, which is due to the random destructive or constructive interferences of the defect reflections with the coherent noise traces, is greatly reduced when using methods 2 and 3 in the corresponding scenarios. Although in this case the defect indications obtained with the stretch-based methods are indeed on average lower than the correct amplitude (and also lower than the ones seen in Figure 19(b) and Figure 21(c) for the same 6 dB defects, but with the 10 dB weld), the ROC curves of Figure 23(c,f) show that the detection performances offered by methods 2 and 3, respectively in the 2nd and 3rd scenarios, are still substantially better than the ones obtained with method 1, so it is still beneficial to use the

26

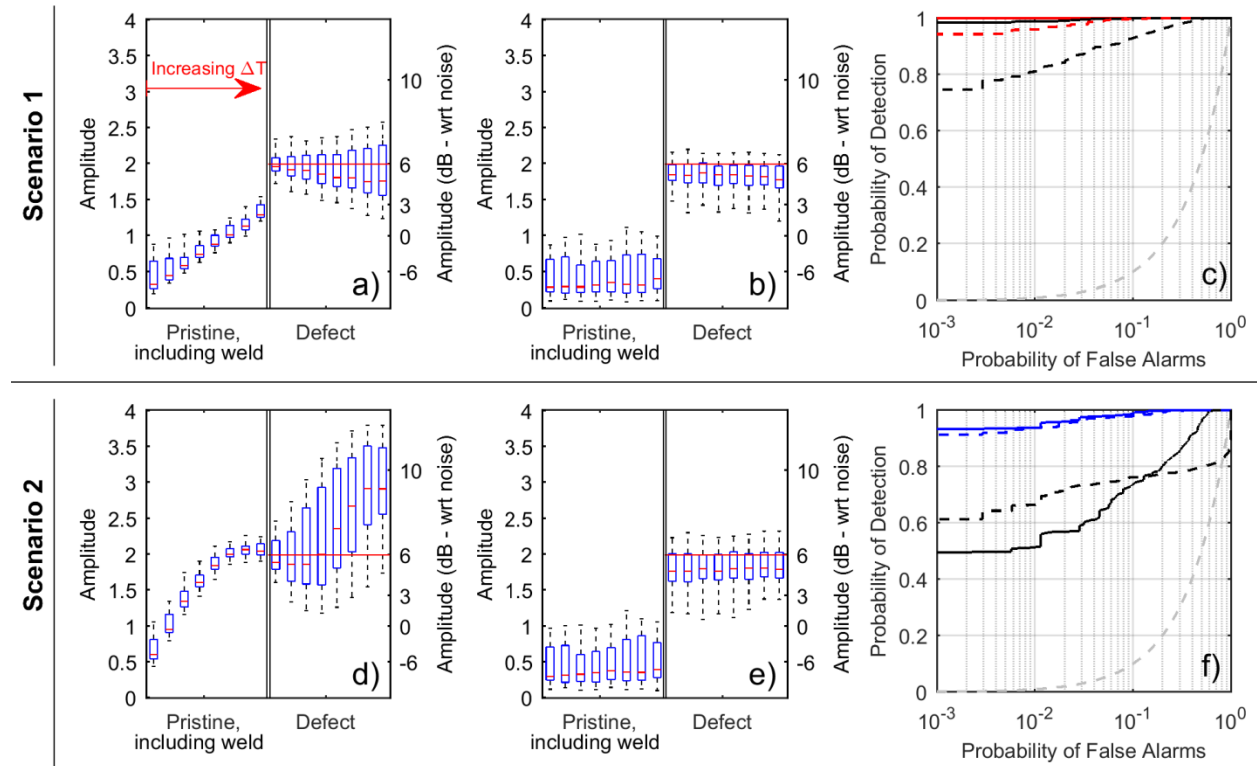compensation techniques, even in the absence of a significant benign reflector in the baseline signal.

Figure 23. Results from signals with synthetic weld at -20 dB wrt to the noise level: a-c) scenario 1; d-f) scenario 2. a,b,d,e) Box plots of the maximum values of residuals (symbols and lines used as in Figure 19, but the amplitude here is normalized to unity at the noise level). a,d) Results from method 1. b) Results from method 2. e) Results from method 3. c,f) ROC curves computed from the signals of scenario 1 (c) and 2 (f), for a defect response amplitude 6 dB above the noise level (lines used as in Figure 22). Note that plots (c,f) are on semi-logarithmic scale.

Conclusions

A new stretch based temperature compensation procedure allowing for both wave velocity and transducer phase response changes has been presented. The procedure is a development of the baseline signal stretch (BSS) technique, and compensates a current signal by minimizing its residual compared to a set baseline. The results with the new method were compared with those obtained using the standard BSS technique on both experimental and numerical signals. For the latter, a series of synthetic signals with different coherent noise levels, feature reflections and defect sizes were generated, the range of noise levels and phase changes being chosen based on initial experiments and prior field experience.

The results from the experimental signals show that the new method successfully gave lower residuals than the standard technique, with a fractional improvement increasing at higher temperature differences between the current signal and the set baseline. For example, the new

method roughly halved the residual between baseline and current signals when the two signals were acquired at temperatures 15 °C apart.

The results from the numerical signals show that when including a weld giving a reflection 10 dB above the coherent noise level, the new method gave roughly 97% probability of detection (POD) for 0.1% probability of false alarm (PFA) for defects giving a reflection 6 dB above the noise level. These results were obtained on signals at two different ranges of temperature differences from the baseline, namely 7 to 28 °C and 35 to 55 °C, with only a very small variation of results between the two. At the same 0.1% false alarm rate, the standard BSS technique yielded only a 23% POD when dealing with temperature differences from 7 to 28 °C, and a 2% POD for the 35 to 55 °C range. It should be noted that most false alarms occurred at the weld location where there is already a significant reflection.

There are cases where the inspected structure either only has features giving reflections lower than the coherent noise, or has no benign features at all over the inspected region. In these cases, there has been a concern that in the process of minimizing the difference between the current and baseline signals, the stretch based compensation procedure would tend to reduce the size of the defect signal, perhaps to below the coherent noise level, and so reduce the probability of its detection. However, the results show that even when the largest benign feature gives a reflection -20 dB wrt the noise level, there is little degradation of performance.

In the numerical study presented here, the effects of changing temperature on the transducer frequency response were simply simulated by applying a constant phase shift across the frequency range of the input toneburst. In some transduction systems, more complex frequency response function changes with temperature may be seen; although it would be possible to model such behaviors, these effects are clearly sensor-specific and would involve several variables. If the method proposed here required improvement with a particular sensor, it would be possible to extend it to the optimization of further variables.

The temperature of some inspected structures may be non-uniform over their length, for example a partially buried pipe, or one missing insulation over some segments. In these cases, as suggested by Galvagni [30], the proposed method may be applied to different segments of the structure in turn, the temperature of each segment being considered approximately uniform.

Acknowledgments

Declaration of conflicting interests

Funding

References

1. Cawley P, Cegla F, Stone M. Corrosion Monitoring Strategies—Choice Between Area and Point Measurements. *J Nondestruct Eval* 2013; 32: 156–163.

2. Cawley P, Lowe M, Alleyne D, et al. Practical long range guided wave inspection-applications to pipes and rail. *Mater Eval* 2003; 61: 66–74.

3. Alleyne DN, Cawley P. The excitation of Lamb waves in pipes using dry-coupled piezoelectric transducers. *J Nondestruct Eval* 1996; 15: 11–20.

4. Nunez Ledesma VM, Perez Baruch E, Demma A, et al. Guided Wave Testing of an Immersed Gas Pipeline. *Mater Eval* 2009; 67: 102–115.

5. Cawley P, Cegla F, Galvagni A. Guided waves for NDT and permanently-installed monitoring. *Insight - Non-Destructive Test Cond Monit* 2012; 54: 594–601.

6. Croxford AJ, Wilcox PD, Drinkwater BW, et al. Strategies for guided-wave structural health monitoring. *Proc R Soc A Math Phys Eng Sci* 2007; 463: 2961–2981.

7. Lu Y, Michaels JE. A methodology for structural health monitoring with diffuse ultrasonic waves in the presence of temperature variations. *Ultrasonics* 2005; 43: 717–731.

8. Konstantinidis G, Wilcox PD, Drinkwater BW. An Investigation Into the Temperature Stability of a Guided Wave Structural Health Monitoring System Using Permanently Attached Sensors. *IEEE Sens J* 2007; 7: 905–912.

9. Clarke T, Simonetti F, Cawley P. Guided wave health monitoring of complex structures by sparse array systems: Influence of temperature changes on performance. *J Sound Vib* 2010; 329: 2306–2322.

10. Weaver RL, Lobkis OI. Temperature dependence of diffuse field phase. *Ultrasonics* 2000; 38: 491–494.

11. Sohn H. Effects of environmental and operational variability on structural health monitoring. *Philos Trans A Math Phys Eng Sci* 2007; 365: 539–60.

12. Croxford AJ, Wilcox PD, Konstantinidis G, et al. Strategies for overcoming the effect of temperature on guided wave structural health monitoring. In: Kundu T (ed) *Health Monitoring of Structural and Biological Systems 2007*. International Society for Optics and Photonics, p. 65321T.

13. Harley JB, Moura JMF. Scale transform signal processing for optimal ultrasonic temperature compensation. *IEEE Trans Ultrason Ferroelectr Freq Control* 2012; 59: 2226–2236.

14. Ha S, Lonkar K, Mittal A, et al. Adhesive Layer Effects on PZT-induced Lamb Waves at Elevated Temperatures. *Struct Heal Monit* 2010; 9: 247–256.

15. Herdovics B, Cegla F. Structural health monitoring using torsional guided wave electromagnetic acoustic transducers. *Struct Heal Monit* 2018; 17: 24–38.

16. Herdovics B, Cegla F. Compensation of phase response changes in ultrasonic transducers caused by temperature variations. *Struct Heal Monit* 2018; (Published online first).

17. Assous S, Rees J, Lovell M, et al. Bandwidth enhancement: Correcting magnitude and

phase distortion in wideband piezoelectric transducer systems. *Advances in Piezoelectric Transducers*, http://www.intechopen.com/books/advances-in-piezoelectric-transducers/bandwidth-enhancement-correcting-magnitude-and-phase-distortion-in-wideband-piezoelectric-transducer (2011, accessed 4 August 2018).

18. Hurst AM, Carter S, Firth D, et al. Real-Time, Advanced Electrical Filtering for Pressure Transducer Frequency Response Correction. In: *Volume 6: Ceramics; Controls, Diagnostics and Instrumentation; Education; Manufacturing Materials and Metallurgy; Honors and Awards*. ASME, p. V006T05A015.

19. Labyed Y, Lianjie Huang. Super-resolution ultrasound imaging using a phase-coherent MUSIC method with compensation for the phase response of transducer elements. *IEEE Trans Ultrason Ferroelectr Freq Control* 2013; 60: 1048–1060.

20. Fawcett T. An introduction to ROC analysis. *Pattern Recognit Lett* 2006; 27: 861–874.

21. Huthwaite P. Accelerated finite element elastodynamic simulations using the GPU. *J Comput Phys* 2014; 257: 687–707.

22. Alleyne DN, Pavlakovic B, Lowe MJS, et al. Rapid, long range inspection of chemical plant pipework using guided waves. In: *AIP Conference Proceedings*. AIP, pp. 180–187.

23. Wilcox PD. Guided-wave Array Methods. *Encyclopedia of Structural Health Monitoring (eds C. Boller, F. Chang and Y. Fujino)*. Epub ahead of print 2009. DOI: 10.1002/9780470061626.shm016.

24. Demma A, Cawley P, Lowe M, et al. The reflection of the fundamental torsional mode from cracks and notches in pipes. *J Acoust Soc Am* 2003; 114: 611–625.

25. Liu C, Dobson J, Cawley P. Efficient generation of receiver operating characteristics for the evaluation of damage detection in practical structural health monitoring applications. *Proc R Soc A Math Phys Eng Sci*; 473. Epub ahead of print 2017. DOI: 10.1098/rspa.2016.0736.

26. Heinlein S, Cawley P, Vogt T. Validation of a procedure for the evaluation of the performance of an installed structural health monitoring system. *Struct Heal Monit*. Epub ahead of print 12 September 2018. DOI: 10.1177/1475921718798567.

27. Wilcox PD, Croxford AJ, Michaels JE, et al. A comparison of temperature compensation methods for guided wave structural health monitoring. In: *AIP Conference Proceedings*. AIP, pp. 1453–1460.

28. Guided Ultrasonics Ltd., https://www.guided-ultrasonics.com/ (accessed 22 August 2018).

29. Heinlein S, Cawley P, Vogt T, et al. Blind trial validation of a guided wave structural health monitoring system for pipework. *Mater Eval* 2018; 76: 1118–1126.

30. Galvagni A. *Pipeline health monitoring*. PhD Thesis, Imperial College London, London, 2013.

31. Goldberg DE, Holland JH. Genetic Algorithms and Machine Learning. *Mach Learn* 1988; 3: 95–99.

32. Han W. A new denoising algorithm for MFL data obtained from seamless pipeline inspection. *Russ J Nondestruct Test* 2008; 44: 184–195.

33. Jarvis R. *Current deflection NDE for pipe inspection and monitoring*. PhD Thesis, Imperial College London, London, 2017.

34. Gridin D, Craster RV, Fong J, et al. The high-frequency asymptotic analysis of guided waves in a circular elastic annulus. *Wave Motion* 2003; 38: 67–90.

35. Yinghui Lu, Michaels JE. Feature Extraction and Sensor Fusion for Ultrasonic Structural Health Monitoring Under Changing Environmental Conditions. *IEEE Sens J* 2009; 9: 1462–1471.

36. Mariani S, di Scalea FL. Predictions of defect detection performance of air-coupled ultrasonic rail inspection system. *Struct Heal Monit* 2018; 17: 684–705.